Check for
updates

Superfluid Drain Vortex

Wandrille Ruffenach[1] · Luca Galantucci[2,3] · Carlo F. Barenghi[2]

Abstract

Drain vortices are among the most common vortices observed in everyday life, yet their physics is complex due to the competition of vorticity's transport and diffusion, and the presence of viscous layers and a free surface. Recently, it has become possible to study experimentally drain vortices in liquid helium II, a quantum fluid whose physics is characterised by the absence of viscosity and the quantisation of the circulation in the superfluid component. Using the Gross–Pitaevskii equation, we make a simple model of the problem which captures the essential physics ingredients, showing that the drain vortex of a pure superfluid consists of a bundle of vortex lines which, in the presence of a radial drain, twist, thus strengthening the axial flow into the drain.

1 Introduction

Quantised vorticity is a distinguishing property of superfluids, indeed hundreds of papers have been written on this subject since Vinen's detection of single quanta of circulation in superfluid helium [1]. It is therefore remarkable that, until recently, very little attention has been dedicated in the superfluid context to *drain vortices* (also called *suction vortices* or *bathtub vortices*). Combining azimuthal motion around an axis with radial/axial inflow into a hole, drain vortices are familiar to everybody because they can be easily created in a kitchen or bathroom sink filled with water. Familiarity is not the same as physical understanding, however: boundaries and a free surface create subtle Ekman layers, drainpipe axial flows and upwellings which, even for water drain vortices, have been studied only recently [2, 3].

✉ Carlo F. Barenghi
   carlo.barenghi@newcastle.ac.uk

1   Département de Physique, École Normale Supérieure de Lyon, 46 Allée d'Italie,
    F 69342, Cedex 07 Lyon, France

2   School of Mathematics, Statistics and Physics, Newcastle University,
    Newcastle upon Tyne NE1 7RU, United Kingdom

3   Istituto per le Applicazioni del Calcolo 'M. Picone', (IAC-CNR), via dei Taurini, 19,
    00185 Roma, Italy

We consider liquid helium (^{4}He) at temperature $T < T_\lambda$ where $T_\lambda = 2.17$ K is the critical temperature at saturated vapour pressure. In this low temperature regime, liquid helium consists of two inter-penetrating fluid components, an inviscid superfluid and a viscous normal fluid, whose proportions strongly depend on T. The normal fluid fraction tends to one for $T \to T_\lambda$ and to zero for $T \to 0$; vice versa, the superfluid fraction tends to zero for $T \to T_\lambda$ and to one for $T \to 0$. (In practice, at $T = 1$ K the superfluid fraction is already more than 99%.)

As mentioned, the key property of the superfluid component is that any vorticity is concentrated in thin vortex lines of fixed circulation $\kappa = h/m$ where h is Planck's constant and m is the mass of one helium atom. Therefore we expect that, in the configuration of a drain vortex, the flow pattern of the normal fluid should be (in the first approximation) similar to that of water, including viscous layers and a continuous vorticity field which fills the system, whereas the vorticity of the superfluid should be confined to a central cluster of vortex lines. However, since the vortex lines scatter the thermal excitations (phonons and rotons) which make up the normal fluid, there should also be a mutual friction force between normal fluid and superfluid components, whose precise effects are difficult to guess. (The friction depends on the density of the vortex lines and their velocity difference with respect to the normal fluid.) We also expect that the flow pattern should depend on whether the drain vortex is created mechanically (e.g., using a propeller) or thermally (e.g., using a heater), as the induced superfluid and normal fluid velocities will be parallel or antiparallel, respectively. Finally, unless the container is very large, details of any fluid reinjection into the system will be important. In summary, the superfluid drain vortex problem contains many physical ingredients which may combine in a nontrivial way, even before considering the presence of a free surface, which may deepen creating a funnelling drainpipe.

Experimentally, the problem has been tackled recently by Yano and collaborators [4–6]. Using a rotor, they created a drain vortex in helium at $T = 1.6$ K (corresponding to a superfluid fraction of 83%). By measuring the attenuation of second sound, they showed that the drain vortex consists of a cluster of approximately 10^4 quantised vortex lines which accumulate in a narrow central region near the axis of symmetry above the drain hole. The experiment was followed up by numerical simulations [7] based on the vortex filament model (VFM). These simulations determined the evolution of seeding vortex lines at nonzero temperatures in the presence of a prescribed normal fluid in the shape of a Rankine vortex with a superimposed constant axial flow into the drain hole.

In this paper we do not try to model Yano's experiments precisely: rather, we try to isolate the essential physics ingredients, leaving aside finite-temperature effects. We consider the superfluid drain vortex problem in its simplest form: a vortex cluster in the presence of a drain flow in a pure superfluid at $T = 0$, in the absence of a free surface. We model the problem using the Gross–Pitaevskii Equation (GPE) for a weakly-interacting gas of bosons [9, 10]. The GPE is idealized for helium (which is a liquid, not a dilute gas), and, since its numerical solution requires the resolution of length scales smaller than the vortex core, our calculation is necessarily limited to small-scale vortex configurations. Still, our model captures the essential physical ingredients, namely the dynamics of vortex lines in a nontrivial three-dimensional

geometry which includes a draining superflow and the presence of boundaries, ingredients which were not accounted in the VFM approach [7].

This paper is articulated as follows: Sect. 2 describes our model and the numerical methods employed and Sect. 3 presents our results.

2 Model

2.1 Governing Equations

It is convenient to write the GPE in dimensionless form. We use the healing length $\xi = \hbar/\sqrt{gmn_0}$ and the speed of sound $c = \sqrt{n_0 g/m}$ as units of length and speed, respectively, $\tau = \xi/c$ as unit of time, the density of a uniform condensate, n_0, as the unit of density, and express the trapping potential in units of the chemical potential gn_0, g being the interaction parameter, m the mass of one atom, and $\hbar = h/(2\pi)$ the reduced Planck's constant. The resulting dimensionless GPE is

$$i\frac{\partial \psi}{\partial t} = -\frac{1}{2}\nabla^2 \psi + |\psi|^2 \psi + V\psi, \tag{1}$$

where $\psi(\mathbf{r}, t)$, $n(\mathbf{r}, t) = |\psi(\mathbf{r}, t)|^2$, $V(\mathbf{r})$, $\mathbf{r}$ and t are the dimensionless wavefunction, density, trapping potential, position and time, respectively. (Hereafter all quantities are meant to be dimensionless.) During the evolution, Eq. (1) conserves the total number of atoms, N, in the volume $\mathcal{V}$ of the system, and the energy, E, given, respectively, by

$$N = \int_{\mathcal{V}} n \, d^3\mathbf{r}, \tag{2}$$

$$E = \int_{\mathcal{V}} \left(\frac{1}{2}|\nabla \psi|^2 + \frac{1}{2}|\psi|^4 + V|\psi|^2\right) d^3\mathbf{r}. \tag{3}$$

We solve the three-dimensional GPE numerically in the computational domain $x_{\min} \le x \le x_{\max}$, $y_{\min} \le y \le y_{\max}$, $z_{\min} \le z \le z_{\max}$ using the 4th order Runge–Kutta method in time and centred differences in space; the spatial discretization consists of N_x, N_y and N_z discretization points in the x, y and z directions, respectively. Convergence is checked by monitoring the conservation laws; for typical time evolutions described in the next section, N and E are conserved with relative errors $(N - N_0)/N_0 \approx 10^{-5}$ % and $(E - E_0)/E_0 \approx 0.05$ % where N_0 and E_0 are the initial values.

2.2 Geometry of the System

For a system whose geometry is described in Fig. 1, we set $V(\mathbf{r}) = V_{\text{trap}}(\mathbf{r})$ in Eq. (1), where the trapping potential $V_{\text{trap}}(\mathbf{r})$ is equal to zero inside the following three regions: (i) a cylinder of radius r_{ad} extending from z_1 to z_2 which represents

Fig. 1 The geometry of our numerical experiments. Top: schematic cross section on the $y = 0$ plane. The yellow and pink regions are the drain hole and the injection annulus, respectively. Bottom: schematic three-dimensional view for $z_3 = z_1$
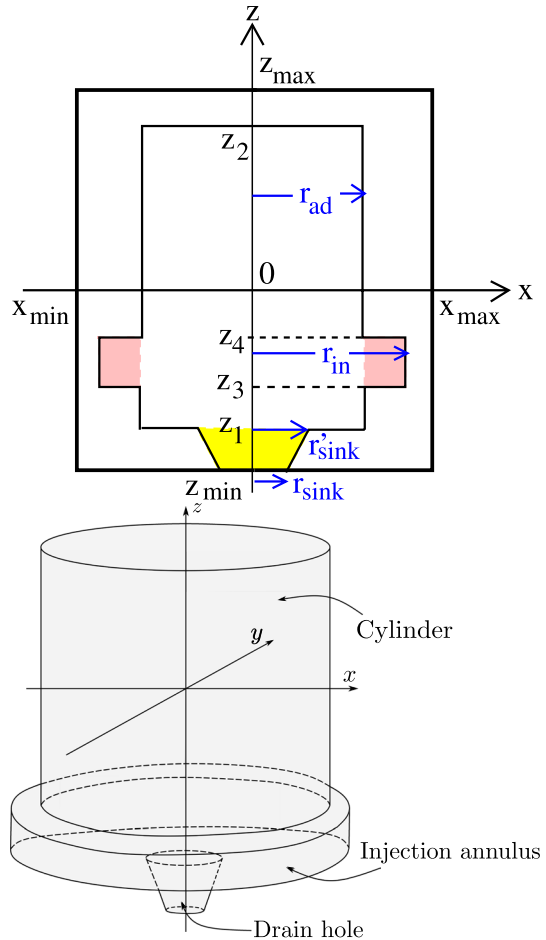
the experimental cell; (ii) a drain hole in the shape of a truncated cone with top radius r'_{sink} and bottom radius r_{sink} extending from z_{min} to z_1; (iii) an injection annulus of inner radius r_{ad} and outer radius r_{in} extending from z_3 to z_4. Outside these three regions, we set $V_{trap}(\mathbf{r}) = 10$ (in units of the chemical potential). This value corresponds to a high potential barrier imposing $\psi = 0$ outside the regions (i) - (iii). In the experiment of Yano and collaborators [4] the injection annulus is at the bottom of the experimental cell, so here we present the results for $z_3 = z_1$ (i.e., the injection annulus is at the bottom of the cylinder).

2.3 Drain and Injection

To model the drain hole, we add a negative imaginary part to the potential $V(\mathbf{r})$ in region (ii) (the truncated cone below the cylinder), setting

$$V(\mathbf{r}) = V_{\mathrm{trap}}(\mathbf{r}) - iV_{\mathrm{sink}}(\mathbf{r}), \tag{4}$$

where $V_{sink}(\mathbf{r})$ is equal to a positive constant V_0 in the drain hole and zero elsewhere. Between t and $t + \Delta t$, this negative imaginary potential removes $\Delta N(t)$ atoms from the drain hole, depleting the density in that region. To see this, we derive [9] from Eq. (1) the modified Euler equation

$$n\left(\frac{\partial \mathbf{v}}{\partial t} + (\mathbf{v} \cdot \nabla)\mathbf{v}\right) = -\nabla p - n\nabla V_{\mathrm{trap}} + \frac{n}{2}\nabla\left(\frac{\nabla^2 \sqrt{n}}{\sqrt{n}}\right), \tag{5}$$

and the modified continuity equation

$$\frac{\partial n}{\partial t} + \nabla \cdot (n\mathbf{v}) = -2nV_{\mathrm{sink}}, \tag{6}$$

where

$$p = \frac{n^2}{2}, \tag{7}$$

is the pressure, $\mathbf{v} = \mathbf{j}/n$ is the velocity, and the current $\mathbf{j}$ is defined as

$$\mathbf{j} = n\mathbf{v} = \frac{i}{2}(\psi \nabla \psi^* - \psi^* \nabla \psi). \tag{8}$$

The last term of Eq. (5) is called the quantum pressure term. By integrating Eq. (8) over the whole volume, we obtain that the rate of loss of particles into the system due to drain potential is given by $-\dfrac{\mathrm{d}N}{\mathrm{d}t} = 2V_0 N_{\mathrm{sink}}(t)$, where $N_{\mathrm{sink}}(t)$ is the number of atoms in the drain hole. The number of atoms $\Delta N(t)$ removed from the drain hole in time Δt is hence, in the first approximation, given by $\Delta N(t) \approx 2V_0 N_{\mathrm{sink}}(t)\Delta t$. As the quantum fluid described by Eqs. (5) and (6) is barotropic, see Eq. (7), the density difference arising from the atoms removal in the drain creates a pressure difference which drives a flow towards the drain (see Sect. 3). In order to conserve the total number of atoms of the system, we add into the injection annulus the same number of atoms $\Delta N(t)$ that we have removed from the drain hole. After time-stepping the wavefunction from $\psi(\mathbf{r}, t)$ to $\psi(\mathbf{r}, t + \Delta t)$, the naive approach would be to change the density in the injection annulus from $n(\mathbf{r}, t + \Delta t)$ to $n'(\mathbf{r}, t + \Delta t) = n(\mathbf{r}, t + \Delta t) + \Delta N/\mathcal{V}_{in}$, where $\mathcal{V}_{in}$ is the volume of the injection annulus. However, we have found that the resulting unphysical small radial discontinuity of the density at the edge of the injection annulus ($r = r_{ad}$) tends to destabilize the solution even at small values of the drain parameter V_0. A more stable injection is obtained if the injected density profile is continuous. Therefore we set $n'(\mathbf{r}, t + \Delta t) = n(\mathbf{r}, t + \Delta t) + f(r)\Delta N(t)$, where the distribution function $f(r)$ is not a step-function but vanishes at $r = r_{ad}$ and $r = r_{in}$, and its volume integral is normalized to one. For simplicity we choose

$$f(r) = \frac{\sin\left[\pi(r - r_{ad})/(r_{in} - r_{ad})\right]}{2(z_4 - z_3)(r_{in}^2 - r_{ad}^2)}, \tag{9}$$

where

$$\int_0^{2\pi} d\theta \int_{z_3}^{z_4} dz \int_{r_{ad}}^{r_{in}} dr\, r f(r) = 1. \tag{10}$$

Other choices of distribution function which guarantee a continuous density profile at the edge of the annulus give a similar drain flow.

Our particle re-injection protocol can physically be interpreted as the inclusion of a source term σ_{in} in the continuity equation Eq. (6), i.e.,

$$\frac{\partial n}{\partial t} + \nabla \cdot (n\mathbf{v}) = -2nV_{sink}(\mathbf{r}) + \sigma_{in}(\mathbf{r}, t), \tag{11}$$

where the production term, $\sigma_{in}(\mathbf{r}, t)$, is nonzero only inside the injection annulus. Since $V_{sink}(\mathbf{r})$ is equal to a constant, V_0, inside the drain hole and vanishes outside it, in order that the number of atoms in the system remains the same, $\sigma_{in}(\mathbf{r}, t)$ must satisfy

$$\int_{\mathcal{V}_{in}} \sigma_{in}(\mathbf{r}, t)\, d^3\mathbf{r} = 2N_{sink}(t)V_0. \tag{12}$$

3 Results

3.1 Ground State

To find the ground state of the system, we start from the Thomas-Fermi approximation, imposing that $\psi_{TF}(\mathbf{r}) = \sqrt{1 - V_{trap}(\mathbf{r})}$ if $V_{trap}(\mathbf{r}) < 1$ and zero otherwise. Without any drain flow or injection, we integrate Eq. (1) in imaginary time, replacing t with $-it$ and we enforce at every time step the condition that the total number of atoms in the system does not change. After few time steps, boundary layers of thickness of the order of the healing length (which is unity in our dimensionless formulation) develop near the boundaries, where the density drops from its bulk value in the interior to zero, and the wavefunction settles down to the desired time-independent state which minimizes the energy.

3.2 Steady Drain Flow

We solve the GPE using the ground state as initial condition, imposing drain flow and injection as described in Sect. 2.3. After an initial transient, we obtain a steady drain flow into the drain hole which is exactly compensated by the

injection of atoms in the annular region, so that the number of atoms in the system remains constantly equal to the initial atom number.

It is interesting to relate V_0 (the amplitude of the imaginary potential in Eq. (4) generating the drain flow) to the quantity which is controlled in the experiment: the flow rate from the injection annulus into the drain hole, Q_{inj}. To do this, we integrate Eq. (11) over the volume $\mathcal{V}_s$ of the drain hole, and define

$$Q_{sink} = \oint_{\Sigma_s} n\mathbf{v} \cdot d\mathbf{S},\tag{13}$$

the flow rate out of $\mathcal{V}_s$, where Σ_s is the surface which encloses $\mathcal{V}_s$. Because of the box-trap boundary conditions, the only flow in and out of $\mathcal{V}_s$ is across the top surface $\overline{\Sigma}_s$ of the truncated cone, i.e., $Q_{sink} = \int_{\overline{\Sigma}_s} n\mathbf{v} \cdot d\mathbf{S}$. We find

$$\frac{dN_{sink}}{dt} + Q_{sink} = -2V_0 N_{sink},\tag{14}$$

In the steady state $Q_{inj} = -Q_{sink}$, hence

$$Q_{inj} = 2N_{sink}^0 V_0.\tag{15}$$

The steady number of atoms in the drain hole N_{sink}^0 is not constant but depends on the potential V_0, implying that the relation between Q_{inj} and V_0, Eq. (15), is not linear. The dependence of N_{sink}^0 on V_0 can be, at least qualitatively, understood employing the Bernoulli equation which can be derived [9] from Eq. (1) neglecting the quantum pressure effects:

$$\frac{1}{2}v_s^2 + n_s = \frac{1}{2}v_c^2 + n_c,\tag{16}$$

where v_s, p_s and v_c, p_c are velocities and pressures, respectively, in the centre of the drain hole just below the cylinder (where the velocity is $\mathbf{v} = -v_s\hat{z}$, $\hat{z}$ being the unit vector in the z-direction and $v_s > 0$) and in the cylinder far away from the drain hole (where $|\mathbf{v}| = v_c \approx 0$). Employing the Bernoulli equation Eq. (16), we obtain

$$v_s = \sqrt{2(n_c - n_s)},\tag{17}$$

where the density in the drain hole is approximately $n_s = N_{sink}^0/\mathcal{V}_s$. In the first approximation, the flux across the top surface $\overline{\Sigma}_s$ of the drain hole is $Q_{inj} = n_s v_s A_s$, where A_s is the area of $\overline{\Sigma}_s$. Using this last relation, the continuity equation Eq. (15) and the Bernoulli relation Eq. (17), we obtain the following expression for N_{sink}^0:

$$N_{sink}^0 = n_c \mathcal{V}_s - \frac{2V_0^2 \mathcal{V}_s^3}{A_s^2},\tag{18}$$

leading to

$$Q_{\mathrm{inj}} = 2V_0 \mathcal{V}_s \left(n_c - \frac{2V_0^2 \mathcal{V}_s^2}{A_s^2} \right). \tag{19}$$

This non-linear relation between Q_{inj} and V_0 can be indeed observed in Fig. 2a (solid black line), where we also plot Eq. (19) (solid yellow line) and its linear approximation (red dashed line) at small V_0: the agreement at small values of V_0 is very good. It is clear that our assumptions in deriving Eq. (19) are valid when V_0 is not too large compared to the chemical potential.

This nonlinear effect is also visible in Fig. 2b where we plot the dependence on the potential V_0 of the averaged radial and axial components of the current, $\bar{j}_r$ and $\bar{j}_z$, respectively, flowing into the drain hole, averaged over a horizontal disk of radius r'_{sink} at $z = (z_3 + z_4)/2$.

Figure 3 shows the steady drain flow pattern in a larger geometry plotted on the xz plane (a) and on the xy plane (b). It is apparent that the radial and axial flows into the drain hole are confined to the bottom of the cylinder, the radial component being stronger than the axial one. This flow pattern is very different from the flow pattern of a viscous drain hole described in Ref. [2], which suffers viscous friction near all boundaries; our drain flow is instead irrotational and

Fig. 2 Top **a**: Steady-state flow rate out of the injection annulus into the cylinder, Q_{inj}, as a function of the amplitude of the complex trapping potential V_0 which generates the drain flow (solid black line). The solid yellow line corresponds to Eq. (19), while the dashed red line shows its linear approximation at small values of V_0 where it agrees very well with the numerical simulation. Bottom **b**: Steady-state averaged radial and axial current, $\bar{j}_r$ (solid red line) and $\bar{j}_z$ (solid black line), respectively, as a function of V_0. The parameters are: $N_x = N_y = 140$, $N_z = 120$, $x_{\min} = y_{\min} = -35$, $x_{\max} = y_{\max} = 35$, $z_{\min} = -30$, $z_{\max} = 30$, $z_1 = -28$, $z_2 = 29$, $z_3 = -28$, $z_4 = -24$, $r_{ad} = 31$, $r_{in} = 34$, $r_{sink} = 3$, $r'_{sink} = 12$
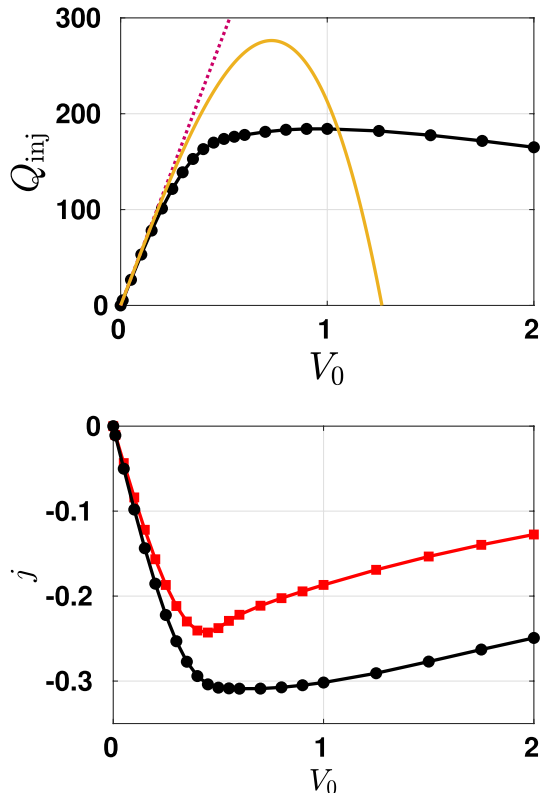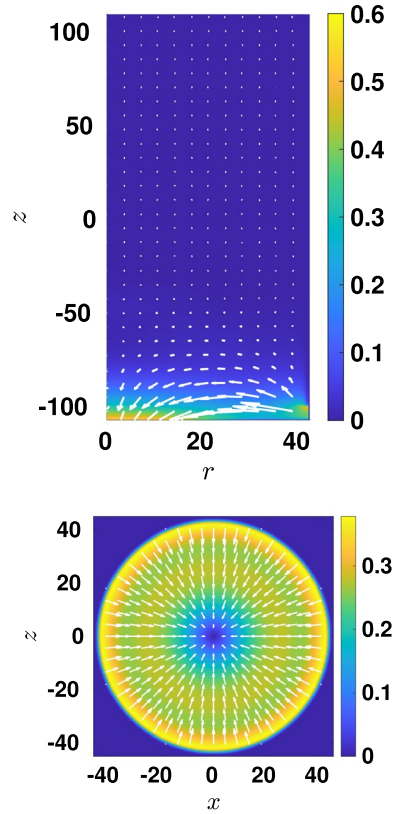
Fig. 3 Top **a** Steady drain flow pattern (in the absence of vortex lines) plotted on the xz plane for $y = 0$. The arrows indicate the direction of the current and the colours represent the current's magnitude. For clarity, only the flow in the cylinder is plotted, ignoring the drain hole and the injection annulus. Bottom **b** Steady drain flow pattern similarly plotted on the xy plane at $z = (z_3 + z_4)/2$. The parameters are: $N_x = N_y = 180$, $N_z = 440$, $x_{min} = y_{rmmin} = -45$, $x_{rmmax} = y_{rmmax} = 45$, $z_{rmmin} - 110$, $z_{rmmax} = 110$, $z_1 = -107$, $z_2 = 109$, $z_3 = z_1$, $z_4 = z_1 + 7$, $r_{rmad} = 31$, $r_{rmin} = 42$, $r_{rmsink} = 5$, $r'_{rmsink} = 30$ and $V^0_{rmsink} = 0.1$

without viscosity. The plot of the pressure distribution (see Fig. 4) confirms that the flow is driven by pressure gradients, as expected.

3.3 Drain Vortex Flow

In the next numerical experiment, we compute the time evolution of a lattice of vortex lines in the presence of a drain flow. We add $N_v = 10$ parallel vortex lines

Fig. 4 Steady drain flow pattern plotted on the xy plane at $z = (z_3 + z_4)/2$. The arrows indicate the direction of the current and the colours correspond to pressure values. Parameters as in Fig. 3
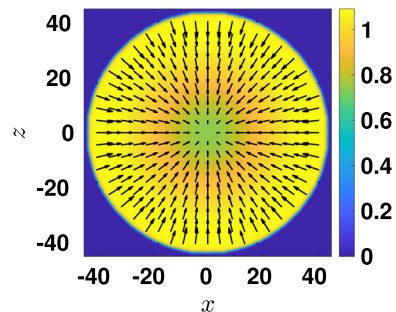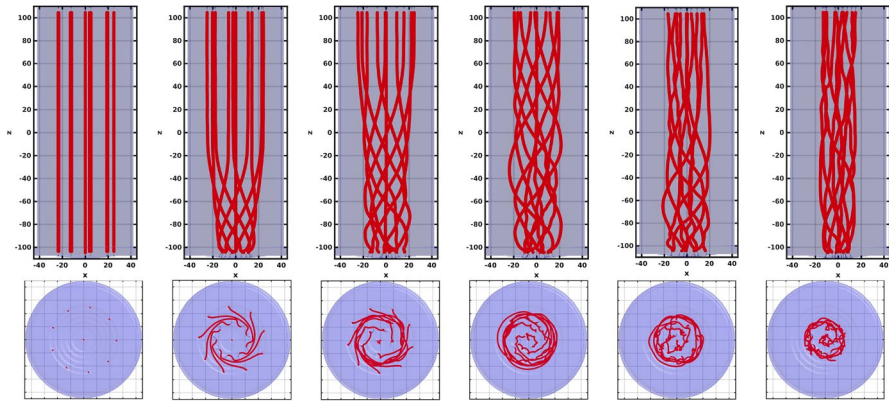
Fig. 5 Snapshots of the vortex configurations at times $t = 0, 320, 640, 960, 1280, 1600$. The parameters are as in Fig. 3
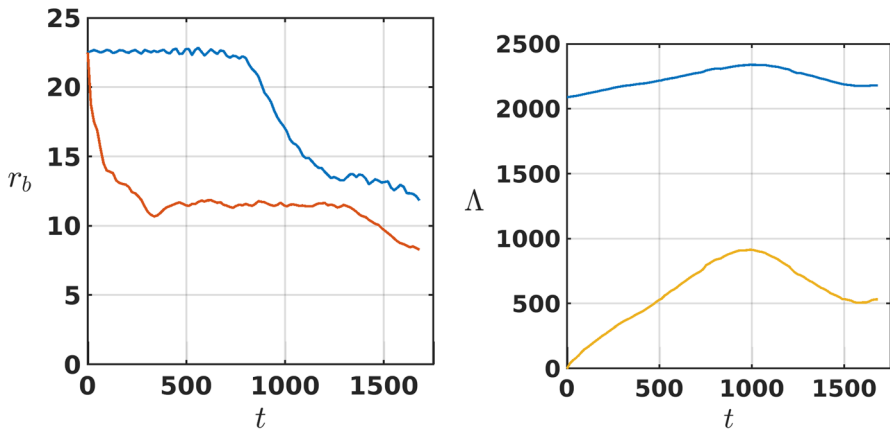

Fig. 6 Left **a**: temporal evolution of the top (blue) and bottom (red) average radius of the vortex bundle r_b; Right **b**: temporal evolution of the total length Λ of the vortex bundle (blue) and its orthogonal projection $\Lambda_\perp$ on a plane perpendicular to the cylinder's axis (yellow). The parameters are as in Fig. 3

aligned along the z-direction which form a small lattice (bundle) of initial radius $r_b = 25$. This vortex imprinting is done in a standard way by multiplying the ground state wavefunction with the approximate wavefunction of a vortex in a homogeneous condensate and let the system then relax in imaginary time.

By integrating in time the GPE, we follow the evolution of the vortex bundle, which is shown in Fig. 5. We find that, since vortex lines are advected by the superflow (Helmholtz's theorem) and since near the bottom of the cylinder the inward radial flow is much stronger than near the top, the lower part of the bundle is sucked radially inwards, towards the centre of the drain hole, while the top part is basically unaffected (this effect is also apparent in Fig. 6a which displays the bundle's radius at two different heights). The quantisation of the superfluid's angular momentum [9,

11] implies that the angular velocity $\Omega(z, t)$ of the bundle at height z and time t is given by the relation $\Omega(z, t) = N_v \kappa / [2\pi r_b^2(z, t)]$. This implies that the bottom parts of the vortex lines which are near the drain hole rotate at larger angular velocity Ω (as r_b is smaller), moving hence "ahead" with respect to the top parts of the vortex lines close to the top of the cylinder: the vortex bundle becomes more and more twisted, as shown in Fig. 5b. As this twist develops, the projection of the total vortex length on a plane orthogonal to the cylinder axis, $\Lambda_\perp$, increases, leading to an increase of the total length, Λ, as shown in Fig. 6b. It takes a finite time for this initial twist to propagate upwards (see Fig. (5)) carried by Kelvin waves on vortices. Once the Kelvin waves reach the top of the cylinder, the bundle's radius, r_b, starts decreasing near the top as well, decreasing $\Lambda_\perp$. However, given the enduring asymmetry of the radial flow (stronger close to the drain hole, negligible near the top of the cylinder), Kelvin waves persist on the vortices, leading $\Lambda_\perp$ to settle to a finite, non-zero value. The dynamics of this rotating, twisted bundle is characterised by vortex reconnections which occasionally scramble the vortex lines, leading to a moderately disordered vortex configuration ($\Lambda_\perp / \Lambda \approx 0.23$ at the end of the simulation) which is still strongly polarised in the z direction.

An important consequence of the twisted nature of vortex lines is that it induces a downwards axial superflow into the drain hole, stronger than the axial superflow caused by the drain hole without vortex lines. Figure 7a and b shows the current on the xz and xy planes, respectively. The presence of the strong axial

Fig. 7 Top **a**: Steady drain flow pattern in the presence of vortex lines plotted on the xz plane for $y = 0$. The arrows indicate the direction of the current and the colours represent the current's magnitude. For clarity, only the flow in the cylinder is plotted, ignoring the drain hole and the injection annulus. Bottom **b**: Steady drain flow pattern plotted on the xy plane at $z = (z_3 + z_4)/2$. The parameters are as in Fig. 3
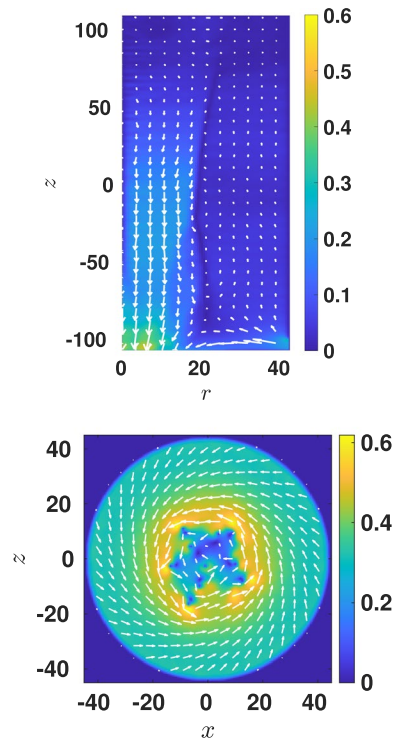
flow towards the drain hole which is induced by the vortices is evident, especially when compared to the axial flow when vortices are absent: compare Figs. 3a and 7a. The azimuthal flow induced by vortices can be observed in Fig. (7)b. As the twist is transported along the z direction by Kelvin waves, it increases the downward axial flow in the upper part of the bundle. Probably this is the mechanism which is responsible for the formation of a central drainpipe funnel when the helium has a top free surface, as observed by Yano and collaborators in their experiments [4]. Further numerical simulations with $N_v = 25$ vortices confirm the scenario which we have described.

4 Discussion and Conclusion

We have used the Gross–Pitaevskii equation to model the superfluid drain vortex in its simplest form: at $T = 0$ (i.e., without any normal fluid and associated viscous effects) and without complications arising from a free surface. We have found that the superfluid drain vortex consists of a moderately disordered twisted bundle of quantised vortex lines (the twist being quantified by the ratio $\Lambda_\perp/\Lambda$). The twist is generated by the radial inflow into the drain, which is stronger near the drain which brings the vortex lines closer to each other. We have also found that the twist of the vortex lines induces a strong central axial flow into the drain; in the presence of a free surface at the top, this axial flow is probably the origin of the dimple, or funnel or drainpipe, which has been observed [4].

Clearly the normal fluid must play an important role in the experiments, and we can speculate that our results shed partial light into it. At small velocities (compared to the speed of sound) and at length scales larger than the healing length, the GPE effectively describes the dynamics of a classical fluid, in particular of the normal fluid, provided we leave aside viscous and friction effects. We can argue therefore that if we start with a normal fluid Rankine vortex at the centre of a cylindrical container and then switch on a drain flow at the bottom of the cylinder, the evolution of the Rankine vortex will be similar the evolution of vortex lines showed in Fig. 5. At the bottom, the radius of the Rankine core will decrease, as fluid moves radially into the drain, leading to faster angular velocity compared to the top which will twist the Rankine core, hence induce an axial current inside it. Of course viscous and friction effects will damp the twist depending on temperature, and to estimate this damping an approach like that used in Ref. [7] is necessary.

The twisted vortex bundle which we report is similar to other twisted vortex states which have been observed in superconductors [12], and, more relevantly, in rotating ^{3}He [13] and large-scale ^{4}He vortex rings [14–16].

Finally, by combining order (the strong axial polarization) with a controlled amount of disorder (induced by the radial drain flow), our results show that this bathtub vortex flow is a promising configuration to develop theoretical tools based on the HVBK equations and Vinen equation [17, 18] to model problems of rotating quantum turbulence [19], ranging from liquid helium counterflow [20, 21] to neutron star glitches [22, 23] to atomic gases [24].

References

1. W.F. Vinen, The detection of single quanta of circulation in liquid helium II. Proc. Roy. Soc. London A **260**, 218 (1961)
2. A. Andersen, T. Bohr, B. Stenum, J. Juul Rasmussen, B. Lautrup, Anatomy of a bathtub vortex. Phys. Rev. Lett. **91**, 104502 (2003)
3. L. Bohling, A. Andersen, D. Fabre, Structure of a steady drain-hole vortex in a viscous fluid. J. Fluid Mech. **656**, 177 (2010)
4. H. Yano, K. Ohyama, K. Obara, O. Ishikawa, Observation of the spiral flow and vortex induced by suction pump in superfluid ^{4}He. J. Phys. Conf. Ser. **969**, 012002 (2018)
5. I. Matsumura, K. Ohyama, K. Sato, K. Obara, H. Yano, O. Ishikawa, Observation of second sound attenuation across a superfluid suction vortex. J. Low Temp. Phys. **196**, 204 (2019)
6. K. Obara, I. Matsumura, N. Tajima, K. Ohyama, H. Yano, O. Ishikawa, Vortex line density of superfluid suction vortex. Phys. Rev. Fluids **6**, 064802 (2021)
7. S. Inui, T. Nakagawa, M. Tsubota, Bathtub vortex in superfluid ^{4}He. Phys. Rev. E **102**, 224511 (2020)
8. K.W. Schwarz, Three-dimensional vortex dynamics in superfluid ^{4}He: homogeneous superfluid turbulence. Phys. Rev. B **38**, 2398 (1988)
9. C.F. Barenghi, N.G. Parker, *A primer on quantum fluids* (Springer, New York, 2016)
10. L. Pitaevskii, S. Stringari, *Bose-Einstein condensation* (Clarendon Press, Oxford, 2003)
11. R.P. Feynman, Application of quantum mechanics to liquid helium, in *Progress in Low Temperature Physics*, vol. 1, ed. C.J. Gorter, North Holland, Amsterdam (1955)
12. R.D. Kamien, Force-free configurations of vortices in high-temperature superconductors near the melting transition. Phys. Rev. B **58**, 8218 (1998)
13. V.B. Eltsov, A.P. Finne, R. Hänninen, J. Kopu, M. Krusius, M. Tsubota, E.V. Thuneberg, Twisted vortex state. Phys. Rev. Lett. **96**, 215302 (2006)
14. D.H. Wacks, A.W. Baggaley, C.F. Barenghi, Coherent laminar and turbulent motion of toroidal vortex bundles Phys. Fluids **26**, 027102 (2014)
15. L. Galantucci, G. Krstulovic, C.F. Barenghi, Friction-enhanced lifetime of bundled quantum vortices, http://arxiv.org/abs/2107.07768 (2021)
16. P. Svancara, M. Pavelka, M. La Mantia, An experimental study of turbulent vortex rings in superfluid ^{4}He. J. Fluid Mech. **889**, A24 (2020)
17. T. Lipniacki, Dynamics of superfluid ^{4}He: two-scale approach. Eur. J. Mech. B/Fluids **25**, 435 (2006)
18. D. Jou, M.S. Mongiovì, M. Sciacca, Hydrodynamic equations of anisotropic, polarized and inhomogeneous superfluid vortex tangles. Physica D **240**, 249 (2011)
19. P.M. Walmsley, A.I. Golov, Rotating quantum turbulence in superfluid ^{4}He in the $T = 0$ limit. Phys. Rev. B **86**, 060518 (2012)
20. C.E. Swanson, C.F. Barenghi, R.J. Donnelly, Rotation of a tangle of quantized vortices in HeII. Phys. Rev. Lett. **50**, 190 (1983)
21. M. Tsubota, T. Araki, C.F. Barenghi, Rotating superfluid turbulence. Phys. Rev. Lett. **90**, 205301 (2003)
22. M.S. Mongiovì, F.G. Russo, and M. Sciacca, A mathematical description of glitches in neutron stars M.N.R.A.S. **469** 2141, (2017)
23. B. Haskell, D. Antonopoulou, and C.F. Barenghi, Turbulent, pinned superfluids in neutron stars and pulsar glitch recoveries, M.N.R.A.S. **499**, 161 (2020)

24. K. Hossain, K. Kobuszewski, M. McNeil Forbes, P. Magierski, K. Sekizawa, G. Wlazłowski, Rotating quantum turbulence in the unitary Fermi gas. Phys. Rev. A **105**, 013304 (2022)